An Improved Estimator of GRID Model for Representing Large Diffeomorphic Deformations

Qian Xie and Anuj Srivastava

Department of Statistics, Florida State University, United States
{qxie,anuj}@stat.fsu.edu

Abstract. The growth by random iterated diffeomorphisms (GRID) model seeks to decompose large deformations, caused by growth, anomaly, or anatomical differences, into smaller, biologically-meaningful components. These components are spatially local and parametric, and are characterized by radial deformation patterns around randomly-placed seeds. A sequential composition of these components, using the group structure of diffeomorphism group, models the cumulative deformation. The actual decomposition requires estimation of GRID parameters from observations of large growth, typically from 2D or 3D images. While past papers have estimated parameters under certain simplifying assumptions, including that different components are spatially separated and non-interacting, we address the problem of parameter estimation under the original GRID model that advocates sequential composition of arbitrarily interacting components. Using a gradient-based approach, we present an algorithm for estimation of GRID parameters by minimizing an energy function and demonstrate its superiority over the past additive methods.

Keywords: Large deformation, GRID model, parameter estimation

1 Introduction

The mathematical and statistical modeling of diffeomorphic deformations over time is an important problem with a variety of applications ranging from medical diagnostics to evolutionary biology. The use of medical images, especially the MRI images of human parts, in studying anatomical structures is a growing area of research by itself. Here one uses 2D and/or 3D images taken across time, species, or specimens to compare to extract salient differences in anatomical structures, and to analyze and model their variations both within and across biological classes. These differences may result from standard biological growth, abnormalities, inter-specimen variability, or other reasons. In terms of image-based analysis of anatomical structures, the study of shapes of anatomical parts has become a central idea. For instance, one can use longitudinal image data for tracking biological growth [11, 9, 19, 4, 3] in fetus brains and evaluating tumor growth. A major difficulty in solving such problems is the high dimensionality of image data. The diffeomorphic deformation when estimated from image

sequences can be very high dimensional and not amenable to standard tools from multivariate statistics. Some current methods simplify this analysis by using simplistic measures like lengths, sizes, or areas as indicators of overall shape changes. Some others use relatively simple geometrical models, such as spheres or ellipsoids, to represent shapes in parametric forms and to study the evolution of parameters during growth.

We start with the basic question of how to represent large deformations in a mathematical framework. There is a large body of work on representing differences in imaged objects using deformations of background space [2, 12, 7, 20, 1, 13]. This approach utilizes diffeomorphisms of the underlying coordinate systems to represent and measure shape and other differences. Let an image be $I : [0,1]^d \to \mathbb{R}$, where $d = 1, 2, 3$. A deformation is then a mapping $\Phi : [0,1]^d \to [0,1]^d$, with the resulting deformed image is $I \circ \Phi : [0,1]^d \to \mathbb{R}$. Thus, a point on an anatomical landmark is always observed with the same color intensity; it simply moves to a different location under the deformation. The goal is to use Φ to model, understand and analyze large deformations. These deformations are typically very high dimensional and do not permit standard statistical analysis directly. Therefore, some tools for reducing dimensionality become important. One can apply some standard dimension reduction algorithms, such as PCA, but it is difficult to interpret the resulting representation in biological terms. Durrleman et al. [5] proposed a parametric way of representing large diffeomorphisms by forcing the instantaneous velocity fields to take a parametric form. One starts with a finite number of so-called control points and for each of them specifies a vector that defines the deformation at that point. The vector field over the whole domain is obtained using a Kernel-based interpolation. This approach provides a data-driven sparse parametric method to estimate the large diffeomorphic deformation.

Motivated by the need for biologically-interpretable decompositions of large deformations, Grenander [8] introduced the Growth as Random Iterated Diffeomorphisms (GRID) model. It highlights the role of gene control in biological growths and uses a combination of local, structured deformations to form the large composite deformations. This model has been studied extensively, but mostly from a perspective of synthesis and asymptotics. Some authors proposed a "thermodynamic limit equation" that approximates the growth pattern in a macroscopic way [16, 15]. Portman et al. [14] further developed the GRID model by analyzing the growth patterns at microscopic levels. In addition to synthesis, one is also interested in the inverse problem where we want to decompose large biological growth into smaller biologically-interpretable units. Grenander et al. [18, 8] studied this inverse problem albeit in a limited context. The estimation of growth components was done in two steps: (1) estimate the full deformation between a pair of images that represents biological growth, (2) estimate parameters for growth components under the GRID model, with a major simplification that different components are spatially local and do not interact with each other. With this assumption, the cumulative growth becomes a simple superimposition of different components and one can use standard projection procedures to esti-

mate component parameters. In this paper we seek a solution to the problem of parameter estimation under the original GRID model, without assuming spatial independence of components. This model is different from Durrleman et al. [5] in the sense that it is the individual diffeomorphisms that take the parametric forms, rather than the instantaneous velocity fields. This results in different local deformations around the focal points. For example, in our method the diffeomorphism around a seed is restricted to be radial while in Durrleman et al. [5] there is no such structure.

The estimation follows the two steps as Grenander et al. [8]. In the first step, the full deformation Φ is estimated using the shape matching technique of [10]. As for the second step, since there is a concatenation of deformation associated with different components, the time-ordering of the components becomes important. Due to the nonlinear effect of compositions, it is not possible to solve for GRID parameters using linear methods. This general estimation problem is posed as an optimization problem with a gradient-based minimization of the cost function. The difficulty of getting trapped in local solutions is handled using clever initializations of the gradient algorithm.

2 Grenander's GRID Model

We start by describing the general GRID model as introduced by Grenander [6]. In this model the overall large deformation is modeled as a composition of a sequence of local, elementary deformations. At time t, the elementary growth is a diffeomorphism $\phi_t : [0,1]^d \to [0,1]^d$ such that the point x moves to $\phi_t(x)$. The full deformation is then expressed in the form of the composition of iterated diffeomorphisms.

$$\Phi_{t_1}^{t_n} \equiv \phi_{t_n} \circ \cdots \circ \phi_{t_2} \circ \phi_{t_1} \tag{1}$$

The next step in the GRID model is to simplify diffemorphic components by expressing each ϕ_t in a parametric form. Here the elementary deformation ϕ_t is: (1) assumed to be centered at a point of activation called a *growth seed* x_{seed}, and (2) the growth around the seed is assumed to be radial. Therefore, it is easier to express this local deformation using polar coordinates centered at the seed x_{seed}: $(r,\tau) \longmapsto (\rho(r,\tau),\tau)$ with $r = 0$ denoting the seed. Furthermore, the model assumes that the change in radial distance can be decomposed into two independent parts: $\rho(r,\tau) = r + R(r)\,A(\tau)$. Here, $A : \mathbb{S}^1 \mapsto R$ is called the angular deformation function (ADF) and $R : \mathbb{R}_+ \mapsto \mathbb{R}_+$ is called the radial deformation function (RDF). These individual deformation functions are allowed to take the following forms:

1. The radial deformation function RDF can be one of the following two types:

$$R(r) = \begin{cases} re^{-r^2/c^2}, & r \geq 0,\ c > 0 \\ (r/c)^{p-1}\, e^{-(r/c)}, & r \geq 0,\ p,\ c > 0\ . \end{cases} \tag{2}$$

   In both cases the deformation is zero at the seed ($r = 0$), increases steadily with r, reaches a peak, and then decreases for a further increase in r. The "zone" of influence of a seed is determined by the parameter c.

2. Similarly, the angular deformation function ADF can also take many forms, including:

$$A(\tau) = \begin{cases} a, & \tau \in \mathbb{S}^1,\ a \in \mathbb{R} \\ ae^{\kappa\cos(\tau-\tau_0)-\kappa}, & \tau \in \mathbb{S}^1,\ a \in \mathbb{R},\ \kappa \geq 0,\ \text{and } \tau_0 \in \mathbb{S}^1 \\ \alpha \sin\left(\frac{2\pi\tau}{\sigma}\right), & \tau \in \mathbb{S}^1,\ \alpha \in \mathbb{R},\ \text{and } \sigma > 0. \end{cases} \quad (3)$$

The first case provides an isotropic deformation, the second provides a unimodal deformation with a well-defined growth/decay direction, while the last one provides a sinusoidal variation.

In this paper we will use $R(r) = re^{-r^2/c^2}$ and will study two choices for ADFs: (1) $A(\tau) = a$, and (2) $A(\tau) = ae^{\kappa\cos(\tau-\tau_0)}$. It has been shown that the resulting ϕ_t is a diffeomorphism as long as $-1 < A(\tau) < 2.2408$ [8]. Each such ϕ_t is now characterized by the following set of parameters: $\theta = [\xi, a, c, \kappa, \tau_0] \in \mathbb{R}^6$, where $\xi \in \mathbb{R}^2$ is the seed location.

Problem Statement: Having chosen the model, the estimation problem can be described as follows. Let Φ represent the observed deformation associated with a growth experiment, observed over a time interval $[0, T]$. The goal now is to estimate n, the number of diffeomorphism components and the associated parameters $\theta_j \in \mathbb{R}^6$ for each $j = 1, 2, \ldots, n$.

This problem has been studied by several papers in the past. However, a common simplifying assumption in the past papers is that different seeds are placed away from each other so that there is no or negligible interaction between the corresponding deformations. In this case, the total displacement field $\Psi(x) = \Phi(x) - x$ can be written as a superposition of the displacements resulting from individual seeds:

$$\Psi_{t_1}^{t_n} \equiv \psi_{t_n} + \cdots + \psi_{t_2} + \psi_{t_1}\ , \quad (4)$$

where $\psi_t(x) = \phi_t(x) - x$. This is a very restrictive assumption and reduces the efficacy of the GRID model. The additive model has several problems, including the fact that the set of diffeomorphisms is not a group under the additive model. In the context of biological growth, it is difficult to interpret growth components under the assumption that there is no spatial interaction between them. Also, as shown in Fig. 1, the results of these different models, composite versus additive models are quite different for the same components. It is also illustrated that, for the composite model, the ordering of components is also important in determining the cumulative deformation. In this paper, we study the problem of parameter estimation under the composite model (Eqn. 1) and compare the results with those obtained under the additive model (Eqn. 4).

3 Our Approach

In this section we formulate the problem of parameter estimation as minimization of a certain objective function. The goal is to estimate difeomorphic components

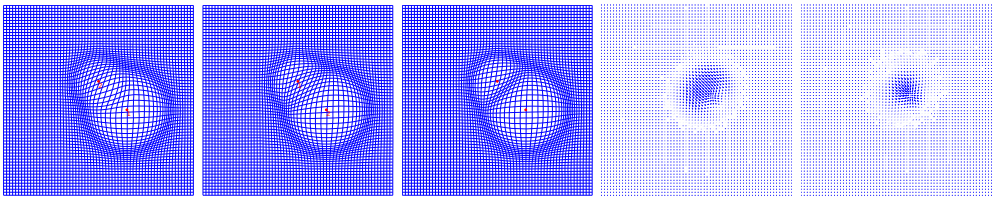

Fig. 1: Cumulative deformation for composite models with: (a) $\Phi = \phi_2 \circ \phi_1$, (b) $\Phi^{'} = \phi_1 \circ \phi_2$, and additive model (c) $\Phi^{''} = x + \psi_1 + \psi_2$, for the same ϕ_1 and ϕ_2. In the remaining panels, we show $\Phi^{'} - \Phi$ (4th panel), and $\Phi^{''} - \Phi$ (5th panel) as vector fields.

$\phi_1,\ \phi_2,\ \ldots, \phi_n$ such that their order composition is as closed to the given Φ as possible. In order words, we can use a distance between Φ and $(\phi_n \circ \cdots \circ \phi_1)$ as the objective function. Although the choice of a geodesic distance in the space of diffeomorphisms (under a suitable Riemannian metric) seems like a natural choice, the use of the $\mathbb{L}^2$ distance simplifies the problem, by forming an energy

$$E = \int_{[0,1]^2} \|\Phi(x) - (\phi_n \circ \cdots \circ \phi_1)(x)\|^2 dx \ . \tag{5}$$

We justify the use of $\mathbb{L}^2$ distance, over the geodesic distance, with the argument that minimization under one distance often leads to a minimizer under the other.

It is rather difficult to solve for all the parameters (for all the seeds) simultaneously. Indeed, the expression for cumulative deformation with just two local deformations gets complicated. Therefore, we take a sequential approach and add one local deformation to the model at a time. Let $\phi^{(k)} = \phi_k \circ \phi_{k-1} \circ \cdots \circ \phi_1$ be the cumulative deformation generated by first k seeds. Define two energy functions associated with this partial inference problem:

$$E^{(k+1)} = \int \left\| \Phi(x) - (\phi_{k+1} \circ \phi^{(k)})(x) \right\|^2 dx$$

and

$$\tilde{E}^{(k+1)} = \int \left\| \Phi(x) - \phi^{(k)}(x) - \psi_{k+1}(x) \right\|^2 dx \ .$$

$E^{(k+1)}$ denotes the energy under the composite model for $k+1$ seeds while $\tilde{E}^{(k+1)}$ denotes a similar energy except that the contribution from the last seed is considered additive. (Since this last seed is additive, it is relatively easier to solve for its parameters by minimizing $\tilde{E}^{(k+1)}$.) Our iterative approach is to solve for the parameters of ϕ_{k+1} to minimize $E^{(k+1)}$, for $k = 1, 2, \ldots, n$, and we will do so using a gradient approach. Similar to any gradient-based solution, the initialization of parameters becomes very important. For the purpose of improving initialization, we will solve for the parameters of ϕ_{k+1} under $\tilde{E}^{(k+1)}$ first and use these values as initial conditions in optimization of $E^{(k+1)}$.

We summarize the iterative procedure for estimating GRID parameters.

Algorithm 1 *Set $k = 0$.*

1. *Given the current estimated parameters for the k-seed composite model, $\{\theta_j\}_k = \{(\xi_j, a_j, c_j, \kappa_j, \tau_{0,j}) \mid j = 1, \ldots, k\}$, compute the cumulative deformation $\phi^{(k)}$.*
2. *Find $\theta_{k+1} = (\xi_{k+1}, a_{k+1}, c_{k+1}, \kappa_{k+1}, \tau_{0,k+1})$ for the $(k+1)^{th}$ seed by minimizing $\tilde{E}^{(k+1)}$. Use these values as initial condition for parameters of the $(k+1)^{th}$ seed.*
3. *For each possible permutation group of the set $\{1, 2, \ldots, k+1\}$, perform the following. Update each set of parameters $\{\theta_j\}_{k+1}$ using the gradient method to minimize $E^{(k+1)}$. Finally, choose the permutation/parameters that result in the minimum $E^{(k+1)}$.*
4. *Test the significance of the $(k+1)^{th}$ seed. If it is found significant, set $k = k+1$ and go to **step 1**; if not, **stop**.*

Note that even though the complexity of the composed deformation $\phi^{(k)}$ and thus $E^{(k)}$ increases with the number of seeds (or local elementary deformations), we still have analytical expressions for the gradients using the chain rule. It is important to note that all the previous seeds are re-estimated/updated as new seeds are added to the deformation. Thus, although this process is iterative, it is not incremental.

We have studied two cases for estimating ADFs:

1. **Constant ADF**: In the first case, we simplify the discussion by first assuming that $A(\tau) = a$ for all $\tau \in \mathbb{S}^1$. In this model, the partial derivatives of $E^{(k)}$ with respect to different parameters of ϕ_j for $j = 1, \cdots, k$ are given by:

$$\frac{\partial E^{(k)}}{\partial \xi_j^r} = \sum_{i=1}^{n} \frac{\partial E^{(k)}}{\partial \phi^{(k)}} \cdot \frac{\partial \phi^{(k)}}{\partial \phi^{(k-1)}} \cdot \frac{\partial \phi^{(k-1)}}{\partial \phi^{(k-2)}} \cdot \cdots \cdot \frac{\partial \phi^{(j+1)}}{\partial \phi^{(j)}} \cdot \frac{\partial \phi^{(j)}}{\partial \xi_j^r}, \quad r = 1, 2 \ ,$$

$$\frac{\partial E^{(k)}}{\partial a_j} = \sum_{i=1}^{n} \frac{\partial E^{(k)}}{\partial \phi^{(k)}} \cdot \frac{\partial \phi^{(k)}}{\partial \phi^{(k-1)}} \cdot \frac{\partial \phi^{(k-1)}}{\partial \phi^{(k-2)}} \cdot \cdots \cdot \frac{\partial \phi^{(j+1)}}{\partial \phi^{(j)}} \cdot \frac{\partial \phi^{(j)}}{\partial a_j} \ ,$$

$$\frac{\partial E^{(k)}}{\partial c_j} = \sum_{i=1}^{n} \frac{\partial E^{(k)}}{\partial \phi^{(k)}} \cdot \frac{\partial \phi^{(k)}}{\partial \phi^{(k-1)}} \cdot \frac{\partial \phi^{(k-1)}}{\partial \phi^{(k-2)}} \cdot \cdots \cdot \frac{\partial \phi^{(j+1)}}{\partial \phi^{(j)}} \cdot \frac{\partial \phi^{(j)}}{\partial c_j} \ .$$

   The different terms needed in these expressions, including $\frac{\partial E^{(j)}}{\partial \phi^{(j)}}$, $\frac{\partial \phi^{(j)}}{\partial \phi^{(j-1)}}$, $\frac{\partial \phi^{(j)}}{\partial \xi_j}$, $\frac{\partial \phi^{(j)}}{\partial a_j}$, and $\frac{\partial \phi^{(j)}}{\partial c_j}$, for $j = 1, \ldots, k$, are given in the appendix. Similar expressions can also be derived for the gradient of $\tilde{E}^{(k)}$ wrt the GRID parameters and those expressions are, as expected, simpler compared to the gradient given above.
2. **Non-isotropic ADF**: In the general case where the ADF is non-isotropic, we represent it using a scaled von-Mises density (the second term in Eqn. 3) and is parameterized by (a, κ, τ_0). For every deformation ϕ_j, the two additional parameters κ_j and $\tau_{0,j}$ are initialized in two steps. First, the ADF is estimated non-parametrically by integrating the deformation along each direction, as was done in [8]. Then, the parameters κ and τ_0 are estimated

from the nonparametric estimate using moment matching. The estimation is similar to estimating the parameters of von-Mises density from a sample by treating the non-parametric estimation as a weighted sample[17]. After these parameters are initialized, they are estimated using the gradient method, similar to the other parameters, with the gradient expression given in the appendix.

The last remaining item in Algorithm 1 is the test of significance of an incremental local deformation. In order to test the significance of the model with one more seed, several general methods for model selection may apply. Possible methods includes partial F test, AIC or BIC, and adjusted R^2. In this paper, a model is selected based on the adjusted R^2. It is a modification of R^2, which denotes the coefficient of determinant, that adjusts for the number of model parameters. Given any two estimated models, the model with the larger value of adjusted R^2 is preferred. In the experiments, we add one more seed if the improvement of adjusted R^2 is larger than a small cutoff value.

Since this method is based on a gradient search, it is difficult to claim a global solution. In principle, the solution obtained in the parameter space is a local one. However, there are some advantages to using this approach. Firstly, since the gradients of the energy function are available analytically, the gradient iterations are computationally fast. Secondly, for relatively small number of seeds in the model, the search over different orderings is efficient and gets us out of several local solutions.

4 Experimental Illustrations

Here we demonstrate the use of our framework for decomposing large cumulative deformations into smaller, parametric components using Algorithm 1. We will use both the simulated and real data to illustrate the estimation process, and will compare our results with those obtained using the additive model.

4.1 Synthetic Data

In order to validate estimation method for the composite model, we perform two experiments on the following types of synthetic data: (1) a 2D deformation with constant ADF, and (2) 2D deformation with non-constant ADF. In these experiments, a cumulative deformation is simulated using Eqn. 1 for an arbitrary number of local deformations, each with arbitrary parameters, and a white Gaussian noise is added at the end to form the observed deformation Φ.

Example 1: Fig. 2 shows the estimation results for the isotropic model. It shows the true underlying deformation (a), made up of $n = 2$ seeds, its noisy observation Φ (b) and several different GRID estimates from the observed Φ (c-e). Firstly, we estimate GRID components as described in Algorithm 1, with the result shown as $\hat{\Phi}_c$ in (e). Then, we reverse the order of two estimated seeds and

try to optimize their parameters, with the result shown as $\hat{\Phi'}_c$ in (c). The result of estimated deformation under the additive model is shown as $\hat{\Phi}_a$ in (d). To highlight the differences between different estimated deformations we also show their differences in the remaining panels. The Table 1 provides a quantification of estimation performance. It compares the energy E and estimated parameters for the three models, with the true values. Since the energy for $\hat{\Phi}_c$ is same as that for true underlying parameters, it shows the superiority of that estimation process described in Algorithm 1.

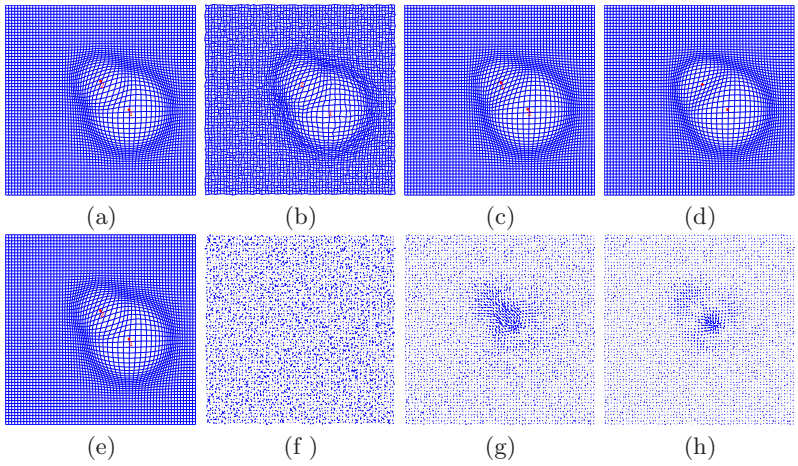

Fig. 2: Experiment with isotropic ADF: (a) synthetic deformation; (b)noisy observation Φ, and different estimated deformations (c) $\hat{\Phi}'_c$; (d)$\hat{\Phi}_a$, and (e)$\hat{\Phi}_c$. The differences (f) $\hat{\Phi}_c - \Phi$, (g)$\hat{\Phi}'_c - \Phi$, and (h)$\hat{\Phi}_a - \Phi$

Model	E	$\xi_1^{(1)}$	$\xi_1^{(2)}$	a_1	c_1	$\xi_2^{(1)}$	$\xi_2^{(2)}$	a_2	c_2
True	**0.0334**	0.6500	0.4500	1.0000	0.1500	0.5000	0.6000	0.8000	0.1000
Estimated $\hat{\Phi}_c$	**0.0334**	0.6500	0.4502	1.0045	0.1498	0.4995	0.6006	0.7947	0.0998
Reverse order $\hat{\Phi'}_c$	0.0576	0.5070	0.5930	0.7072	0.0956	0.6478	0.4525	1.0108	0.1527
Additive $\hat{\Phi}_a$	0.0548	0.6496	0.4507	1.0262	0.1501	0.5172	0.5827	0.7352	0.1004

Table 1: Estimation results for Example 1.

Example 2: Similarly, Fig. 3(a) shows an experiment involving seeds with non-isotropic ADFs. In this case we show the synthetic deformation (a) , its noisy version Φ (b), and the estimated deformation under the composite model $\hat{\Phi}_c$ (c). For further evaluation of this estimation, we show the true displacement

$\Psi(x) = \Phi(x) - x$ (d) and the estimated displacement $\hat{\Psi}$ (e).

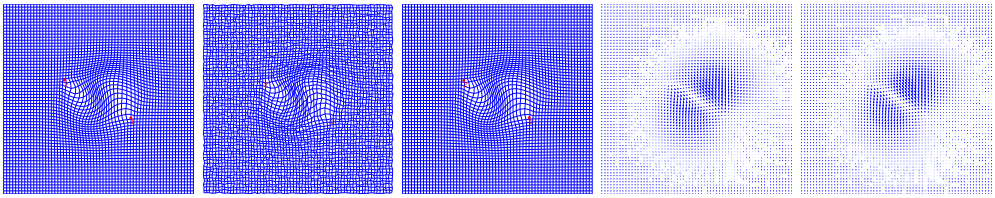

(a) (b) (c) (d) (e)

Fig. 3: Experiment with non-isotropic ADF: (a)synthetic deformation; (b) noisy observation Φ; (c) estimated deformation map $\hat{\Phi}$; (d)true displacement field Ψ; (e)estimated displacement field $\hat{\Psi}$

Model	E	$\xi_1^{(1)}$	$\xi_1^{(2)}$	a_1	c_1	$\xi_2^{(1)}$	$\xi_2^{(2)}$	a_2	c_2
True	0.0330	0.6700	0.4000	1.0000	0.2000	0.3200	0.6000	1.0000	0.2000
Composite	0.0333	0.6677	0.4014	1.0004	0.1975	0.3233	0.5980	1.0248	0.1948
		κ_1	$\tau_{0,1}$			κ_2	$\tau_{0,2}$		
True		2.0000	2.3562			5.0000	5.4978		
Composite		1.9200	2.3379			4.9050	5.4865		

Table 2: Estimation Results for Example 2.

Ensemble Results: Beyond individual examples, we have exhaustively compared performances of the composite and the additive models using many realizations. Here we use 20 sets of data that are simulated from the 2D composite model with constant ADF and the parameters are then estimated using both the models. The results are summarized in Fig. 4. Panel (a) is a histogram of which model, composite or additive, is closer to the true deformation. Positive number indicates that the composite model outperforms the additive one, and vice-versa. We can see that for most data sets the composite model outperforms the additive model. Panel (b) presents a close up view of the parameter biases and variances. Each line represents the bias for one parameter. If the estimates equals the true parameters, the line will be all horizontal lines with $y = 0$. The top plot shows the biases from the additive model and the bottom one is for the composite model. The lines for composite model are all around zero with the ones for additive model having larger variation.

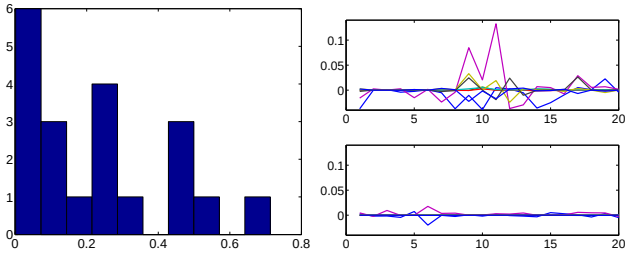

Fig. 4: (a) Relative errors under two models: $\frac{\|\hat{\Phi}_a - \Phi\| - \|\hat{\Phi}_c - \Phi\|}{\|\hat{\Phi}_a - \Phi\|}$; (b) Parameter estimation bias: top: $\hat{\theta}_a - \theta$, bottom: $\hat{\theta}_c - \theta$.

4.2 Estimation of GRID Component for Image Data

This method is applied to analysis of differences in human brains observed using MRI scans. In this case we perform the following experiment. We take two image scans as I and J, which are two slices of MRI of the same z coordinates from different subjects, and use a shape-based technique [10] to estimate a cumulative deformation Φ from I to J. This Φ is in the set of diffeomorphisms from $[0,1]^2$ to itself and minimizes a certain cost function involving $I \circ \Phi$ and J. Then, we use Algorithm 1, to estimate components of this deformation under the GRID model. We present two examples of this idea.

Example 1: Fig. 5 shows an example of images I and J and the deformation Φ that deforms I to match with J. In addition to plotting the maps $x \mapsto \Phi(x)$ as a surface mesh, one can also plot the displacement vector field $\Psi(x) = \Phi(x) - x$ for better visualization. Shown in the remaining panels are the estimated displacement vector $\hat{\Psi}$, showing the ordered sequence of displacement fields with the GRID components that were found using Algorithm 1, and a couple of ways of comparing the estimated deformations with the true deformations.
Example 2: Fig. 6 shows another example of estimating GRID parameters for deformation estimated from MRI images.

5 Conclusion

In this paper we have proposed a method to decompose and estimate the parameters in GRID based decomposition of anatomical deformations. The method preserves the iterative structure of the GRID model and gives an analytical form of the gradient for parameter estimation. Experimental results show that impacts from faraway seeds can be approximated by additive seeds model and composite model can not add much to it; however, as for seeds that are close to each other and have interaction, our method improves the estimation for large deformation as well as the model parameters.

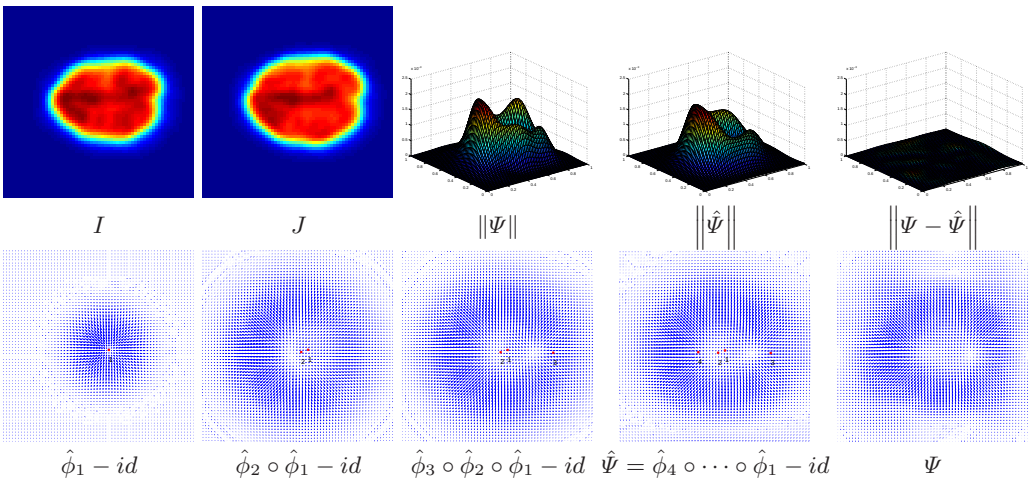

Fig. 5: Estimation of GRID components for deformation between MRI images.

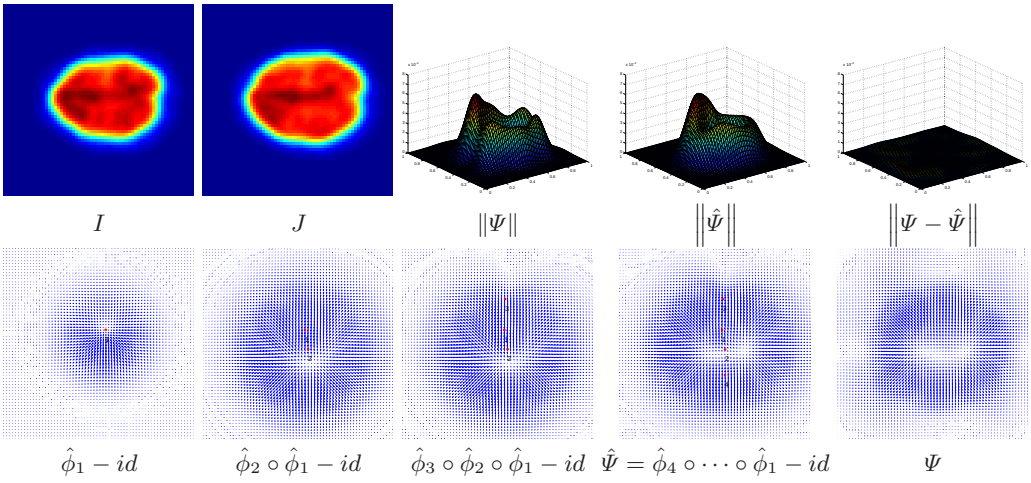

Fig. 6: Estimation of GRID components for deformation between MRI images.

References

1. Andresen, P.R., Nielsen, M.: Non-rigid registration by geometry-constraint diffusion. In: MICCAI. vol. 1679, pp. 533–543 (1999)
2. Arsigny, V., Pennec, X., Ayache, N.: Polyaffine transformations: a new class of diffeomorphisms for locally rigid or affine registration. In: Proc. Nat. Acad. Sci. vol. 90 (1993)

3. Chaplain, M.A.J.: Mathematical modeling of tumor growth. Springer, Seires: Interdisciplinary Applied Mathematics (2006)
4. Clatz, O., Bondiau, P.Y., Delingette, H., Malandain, G., Sermesant, M., Warfield, S.K., Ayache, N.: In silico tumor growth: application to glioblastomas. In: MICCAI. vol. 3217, pp. 337–345 (2004)
5. Durrleman, S., Prastawa, M., Gerig, G., Joshi, S.: Optimal data-driven sparse parameterization of diffeomorphisms for population analysis. In: Inf. Process. Med. Imaging, vol. 22, pp. 123–134 (2011)
6. Grenander, U.: On the mathematics of growth. Quart. of Appl. Math. 65, 205–257 (2007)
7. Grenander, U., Miller, M.I.: Computational anatomy: an emerging discipline. Quart. Appl. Math LVI(4), 617–694 (1998)
8. Grenander, U., Srivastava, A., Saini, S.: A pattern-theoretic characterization of biological growth. IEEE Trans. Med. Imaging 26(5), 648–659 (2007)
9. Kansal, A.R., Torquato, S., IV, G.R.H., Chioccaeb, E.A., Deisboeck, T.S.: Simulated brain tumor growth dynamics using a three-dimensional cellular automaton. J. Theor. Biol. 203, 367–382 (2000)
10. Kurtek, S., Klassen, E., Ding, Z., Jacobso, S., Jacobson, J., Avison, M., Srivastava, A.: Parameterization-invariant shape comparisons of anatomical surfaces. IEEE Trans. Med. Imaging 30(3), 849–858 (2011)
11. Ling, Y., He, B.: Entropic analysis of biological growth models. IEEE Trans. Biomed. Eng. 40(12), 1193–1200 (1993)
12. Miller, M., Christensen, G., Amit, Y., Grenander, U.: Mathematical textbook of deformable neuronatomies. Proc. Nat. Acad. Sci. 90(24), 11944–11948 (1993)
13. Miller, M.I., Younes, L.: Group actions, homeomorphisms, and matching: a general framework. Int. J. Comput. Vision 41(1/2), 61–84 (2001)
14. Portman, N., Grenander, U., Vrscay, E.R.: Direct estimation of biological growth properties from image data using the "grid" model. In: ICIAR '09. vol. 5627, pp. 832–843 (2009)
15. Portman, N., Grenander, U., Vrscay, E.R.: Grid macroscopic growth law and its application to image inference. Quart. Appl. Math. pp. 227–260 (2011)
16. Portman, N., Vrscay, E.R.: Existence and uniqueness of solutions to the grid macroscopic growth equation. Appl. Math. Comput. 217(21), 8318–8327 (2011)
17. Sra, S.: A short note on parameter approximation for Von Mises-Fisher distributions and a fast implementation of $i_s(x)$. Computational Stat. to appear (2009)
18. Srivastava, A., Saini, S., Ding, Z., Grenander, U.: Maximum-likelihood estimation of biological growth variables. In: EMMCVPR'05. vol. 3757, pp. 107–118 (2005)
19. Swanson, K.R., Bridge, C., Murray, J., Jr, E.C.A.: Virtual and real brain tumors: using mathematical modeling to quantify glioma growth and invasion. J. Neurol. Sci. 216(1), 1–10 (2003)
20. Trouvé, A.: Diffeomorphisms groups and pattern matching in image analysis. Int. J. Comput. Vision 28(3), 213–221 (1998)

A Gradient Expressions

The terms, $\frac{\partial E^{(j)}}{\partial \phi^{(j)}} \in R^{1\times d}$, $\frac{\partial \phi^{(j)}}{\partial \phi^{(j-1)}} \in R^{d\times d}$, $\frac{\partial \phi^{(j)}}{\partial \xi_j} \in R^{d\times d}$, $\frac{\partial \phi^{(j)}}{\partial a_j}$, and $\frac{\partial \phi^{(j)}}{\partial c_j} \in R^{d\times 1}$, that are required in gradient computation are given as follows.

$$\frac{\partial E^{(j)}}{\partial \phi^{(j)}} = 2\left(\phi^{(j)} - \Phi\right) \ ,$$

$$\frac{\partial \phi^{(j)}}{\partial \phi^{(j-1)}} = a_{j-1} \cdot \exp\left(-\left(\phi^{(j-1)} - \xi_{j-1}\right)^2 / c_{j-1}^2\right) -$$

$$2a_{j-1} \cdot (\phi^{(j-1)} - \xi_{j-1})^2 / c_{j-1}^2 \cdot \exp\left(-\left(\phi^{(j-1)} - \xi_{j-1}\right)^2 / c_{j-1}^2\right) + 1 \ ,$$

$$\frac{\partial \phi^{(j)}}{\partial \xi_j} = a_j \cdot \exp\left(-\left(\phi^{(j-1)} - \xi_j\right)^2 / c_j^2\right) \cdot \left(2\left(\phi^{(j-1)} - \xi j\right)^2 / c_j^2 - 1\right) \ ,$$

$$\frac{\partial \phi^{(j)}}{\partial a_j} = (\phi^{(j-1)} - \xi_j) \cdot \exp\left(-\left(\phi^{(j-1)} - \xi_j\right)^2 / c_j^2\right) \ ,$$

$$\frac{\partial \phi^{(j)}}{\partial c_j} = 2a_j \cdot \exp\left(-\left(\phi^{(j-1)} - \xi_j\right)^2 / c_j^2\right) \cdot \left(\phi^{(j-1)} - \xi_j\right)^3 / c_j^3 \ .$$

When the ADF takes parametric forms of the second type, the gradient of the energy function with respect to the two parameters κ_j and $\tau_{0,j}$ for $j = 1, \cdots, k$ is calculated in the similar way as the other parameters. The partial derivatives from the one time deformation is shown as below.

$$\frac{\partial \phi^{(j)}}{\partial \kappa_j} = a_j \cdot \exp\left(\kappa_j \cos\left(\tau - \tau_{0,j}\right) - \kappa_j\right) \cdot$$

$$\left(\phi^{(j-1)} - \xi_j\right) \cdot \exp\left(-\left(\phi^{(j-1)} - \xi_j\right)^2 / c_j^2\right) \cdot \left(\cos(\tau - \tau_{0,j}) - 1\right) \ ,$$

$$\frac{\partial \phi^{(j)}}{\partial \tau_{0,j}} = a_j \cdot \exp\left(\kappa_j \cos\left(\tau - \tau_{0,j}\right) - \kappa_j\right) \cdot$$

$$\left(\phi^{(j-1)} - \xi_j\right) \cdot \exp\left(-\left(\phi^{(j-1)} - \xi_j\right)^2 / c_j^2\right) \cdot \kappa_j \cdot \sin\left(\tau - \tau_{0,j}\right) \ .$$